High Capacity Pb(II) Adsorption Characteristics onto Raw- and Chemically Activated Waste Activated Sludge

*AUTHOR NAMES: B. van Veenhuyzen, S. Tichapondwa, C. Hörstmann, E. Chirwa, H. G. Brink**

AUTHOR ADDRESS: Department of Chemical Engineering, Faculty of Engineering, Built Environment and Information Technology, University of Pretoria, Pretoria, Private Bag X20, Hatfield, 0028, South Africa

ABSTRACT

The Pb(II) adsorption characteristics of chemically activated waste activated sewage sludge (WAS) were compared to raw WAS. Adsorption kinetics and equilibrium isotherm parameters were fit using classic adsorption models. HCl and H_2SO_4 activation terminated any significant sludge-based adsorption. Raw and $ZnCl_2$ activated WAS displayed Langmuir adsorption capacities of 307 mg/g and 274 mg/g, respectively. Surface characterization revealed that chemical activation with $ZnCl_2$ increased the BET surface area for raw WAS from 0.97 m^2/g to 1.78 m^2/g, but did not significantly change the surface structure. FTIR analyses and XPS were used to further investigate the nature of lead binding. The relationships between equilibrium ion concentration and Pb(II) adsorption suggest cationic exchange with hydrogen, calcium, and zinc as a significant mechanism of Pb(II) removal alongside electrostatic attraction. The pH_{PZC} was determined as 2.58 and 2.30 for $ZnCl_2$ activated WAS and raw WAS respectively. HNO_3 and $Ca(NO_3)_2$ demonstrated sufficient elution properties for WAS recovery.

For authentic industrial effluent both raw and $ZnCl_2$ activated WAS displayed Pb(II) removal behaviour comparable to simulated Pb(II) solutions. In comparison with modified and unmodified sludges from literature, this study demonstrates the auspicious potential of raw WAS as an effective Pb(II) adsorbent independent of pyrolytic or chemical activation.

KEYWORDS: Adsorption, Chemical activation, Lead, Sewage sludge, Sludge based adsorption

1. INTRODUCTION

Lead pollutants enter the environment through industrial activities such as mining, smelting, and lead battery processing. The presence of lead in water is problematic due to its highly toxic nature and its tendency to accumulate in ecosystems [1].

Conventional heavy metal removal techniques used to remove aqueous lead include adsorption, membrane filtration, electrodialysis, precipitation, and ion exchange [2–5]. Adsorption has proven to be an efficient and cost-effective means of removing aqueous lead ions from polluted water [6] using materials such as biomass, clay, bentonite, zeolite, and activated carbon [7]. Solid wastes are increasingly seen as attractive, sustainable sources for heavy metal adsorption materials, including agricultural wastes [7–9] and industrial wastes [10–13].

Activated carbons are the most commonly employed adsorption material and can be obtained from an array of organic wastes. In spite of this they are still considered relatively expensive [14].

Manufacturing activated carbon or biochar by the pyrolysis of sewage sludge has gained attention as a promising means to produce inexpensive biosorbents from an abundant material while reducing the landfill burden of municipal wastewater treatment plants [6,15–18], however the release of various heavy metals during the reuse of sludge derived activated carbons [19] and the sensitivity of the material properties to solution characteristics [20] can be cited as a cause for concern [19]. The chemical activation processes used in sludge derived biochar also produce chemical wastes in the form of acid/base residues or metal compounds [14].

Several studies have looked into the application of sludge-derived biochar for Pb(II) adsorption [21–25], while others have enhanced biochar adsorption properties with physical activation [26] and chemical activation [23,24,26–30]. In addition, sewage sludge-derived adsorbents that have not undergone pyrolytic processes have been employed for Pb(II) removal including dried, raw waste activated sewage sludge (WAS) [20] and chemically modified WAS [31].

WAS typically consists of a heterogeneous variety of organic and inorganic compounds, microbes and debris [32]. The properties of the sludge vary according to the process from which they are sourced. This sludge is typically obtained from settling tanks that follow secondary wastewater treatment processes such as aeration tanks and trickle filters.

To improve adsorption properties in sludge-based adsorbents, various methods of chemical activation have been studied. Chemicals used for activation prior to pyrolysis typically include H_2SO_4 [16], $ZnCl_2$ [6,19,33], HCl [33,34], KOH, and H_3PO_4 [6]. These compounds catalyze dehydration reactions, resulting in development of porous structures within the carbon [35] that facilitate better adsorption.

This study investigates whether WAS can be employed as an adsorbent without the need of any energy intensive pyrolytic processes and whether chemical activation by commonly used HCl, H_2SO_4 or $ZnCl_2$ significantly improve Pb(II) adsorption. The investigations initiated a kinetic study that included the fitting of pseudo-order models, after which less effective adsorbents were excluded from further experimentation. Particle characterization was thereafter undertaken to examine the properties of the WAS and what effect chemical activation or adsorption had on those properties. Adsorption equilibria were studied, and several adsorption isotherm models were fitted to the data. Subsequently, regeneration studies using HNO_3 and $Ca(NO_3)$ were performed. Finally, to assess the potential of the adsorbents to industrial application, the effectiveness of the adsorbent at treating *bona fide* industrial effluent from an automotive battery recycling plant was assessed in equilibrium batch adsorption experiments.

2. MATERIALS AND METHODS

2.1. Materials preparation

WAS was obtained from a wastewater treatment plant south of Pretoria, South Africa, and dried for three days at 70 °C. For chemical activation, 6 g samples of dried unactivated WAS were wet with 60 mL of activating agent. Zinc chloride [27], hydrochloric acid [36], and sulfuric acid [37] were separately used for WAS activation. Concentration, dilution volumes, and pH of the agents can be found in Table 1. After 1 h, the mixtures were diluted, centrifuged, and rinsed. The volume of water used for washing the adsorbents is presented in Table 1. The activated WAS was thereafter dried overnight at 70 °C.

Table 1. Concentration of agents used to chemically activate secondary sludge, as well as the mixture pH before drying the activated WAS and the amount of water used in washing activated WAS.

Activating agent	Concentration	pH of water after washing	Water used for washing (mL)
$ZnCl_2$	167 g/L	6.05	425
HCl	32 % m/m	2.31	480
H_2SO_4	98 % m/m	2.64	1500

Once dried, both the raw and activated WAS were crushed with a mortar and pestle and sieved to ensure a particle size ≤ 300 µm. A 10 000 mg/L $Pb(NO_3)_2$ as Pb solution was prepared as a source of aqueous lead adsorbate.

2.2. Adsorption kinetics experiments

A series of experiments were carried out to investigate the adsorption kinetics of the raw WAS and chemically activated WAS. Batch adsorption was employed at room temperature using 0.5 g/L adsorbent prepared in 200 mL reactors containing Pb(II) in solution with concentrations ranging from 10 – 50 mg/L Pb(II).

The batch reactors were sampled at various time intervals and passed through 0.45 µm syringe filters. The concentration of aqueous lead remaining in solution was measured with a Perkin Elmer AA400 atomic absorbance spectrophotometer (Perkin Elmer, Waltham, Massachusetts).

The mass of aqueous lead adsorbed onto WAS, Q, was calculated using Equation *1*:

$$Q = \frac{(C_0 - C)V}{W} \quad 1$$

Where Q is in mg/g, C_0 and C are respectively the initial and sampled bulk concentrations in mg/L, W is the adsorbate mass in g, and V is the volume of the batch reactor in L. The sampled adsorptions were fit to a pseudo-first-order isotherm described in Equation 2 [38], a two-phase pseudo-first order isotherm in Equation 3 [39], and a pseudo-second-order isotherm in Equation 4 [38]:

$$\mathrm{Q}(t) = Q_e[1 - exp(-k_1 t)] \quad 2$$

$$Q(t) = Q_{e,fast}\left[1 - exp\left(-k_{1,fast}t\right)\right] + Q_{e,slow}\left[1 - exp\left(-k_{1,slow}t\right)\right] \quad 3$$

$$Q(t) = \frac{Q_e^2 k_2 t}{1 + Q_e k_2 t} \quad 4$$

Here, Q_e is the equilibrium value of adsorbed Pb(II) in mg/g, t is time in min, k_1 and k_2 are the pseudo-first and pseudo-second order rate constants respectively in 1/min and g/(mg·min). In Equation 3, the sum of $Q_{e,fast}$ and $Q_{e,slow}$ gives the overall equilibrium adsorption capacity.

2.3. Mass Transfer Studies

Adsorption proceeds as a series of mass transfer steps in which adsorbate is transported by diffusion from the bulk of the liquid through a stagnant boundary layer to the external surface of the adsorbent – external mass transfer (EMT). Subsequently, the adsorbate is transported diffusionally through the pores of the adsorbent – internal mass transfer (IMT) – to the active adsorption sites on the surface. Finally, the adsorption takes place by either chemisorption or physisorption onto the surface of the adsorbent. The rate of the process is determined by the slowest step/s in the process [40]. The EMT

model assumes that the surface concentration on the adsorbent tend to zero at initiation of the adsorption experiments, i.e. immediately after adsorbent was introduced. This model is mathematically described by equations

$$\frac{\partial C_B}{\partial t} = -k_f \frac{a}{V}(C_B) \quad (5)$$

$$\ln \frac{C_t}{C_0} = -k_f \frac{a}{V} t \quad (6)$$

where C_B is the bulk adsorbate concentration. By fitting the linear curve of $\ln(C_t/C_0)$ against time (for $t \to 0$), and calculating the total area of adsorbent to reactor volume ratio (a/V) using Equation *7*, the mass transfer coefficient (k_f) can be estimated for the different adsorbent systems investigated.

$$\frac{a}{V} = \frac{6W}{\rho d V} \quad (7)$$

The IMT of an adsorbate within an adsorbent, modelled as a sphere with radius r and constant effective adsorbate diffusivity D_e, can be described by the Crank model in Equation 8 [41]:

$$\frac{\partial Q}{\partial t} = \frac{D_e}{r^2}\frac{\partial}{\partial r}\left(\frac{r^2 \partial Q}{\partial r}\right) \quad (8)$$

The analytical solution of Equation *8* can be expressed by Equation 9 [41]

$$\frac{Q}{Q_{max}} = \frac{6}{\pi^2}\sum_{n=1}^{\infty}\frac{1}{n^2}\exp\left(\frac{-D_e n^2 \pi^2 t}{r^2}\right) \quad (9)$$

Equation 9 provides a method to estimate the mass of adsorbate adsorbed as a function of time assuming internal mass transfer as the rate limiting step in the process. Due to the infeasibility of the sum to infinity in Equation 9, simplifications for different experimental times are indicated in Equation 10 [41].

$$\frac{Q}{Q_{max}} = \begin{cases} 6\left(\frac{D_e t}{R^2}\right)^{\frac{1}{2}}\left[\pi^{-\frac{1}{2}} - \left(\frac{1}{2}\right)\left(\frac{-D_e t}{R^2}\right)^{\frac{1}{2}}\right], & \frac{Q}{Q_{max}} < 0.8 \\ 1 - \frac{6}{\pi^2}\exp\left(\frac{-D_e \pi^2 t}{R^2}\right), & \frac{Q}{Q_{max}} \geq 0.8 \end{cases} \quad (10)$$

Once the EMT and IMT parameters (D_e and k_f) have been successfully estimated, the influence of these parameters on the system can be estimated using the dimensionless Biot number for mass transfer (Equation 11). The Bi number provides a criterion for the relative influence of EMT and IMT effects on the adsorption system. Bi > 100 indicates a predominantly IMT limited system, while Bi < 100 indicates that the adsorption process is controlled by EMT [42].

$$\mathrm{Bi} = \frac{k_f d}{D_e} \qquad 11$$

2.4. Characterization of adsorbents

Particle size distribution was determined using a MastersizerHydrosizer 3000 (Malvern Instruments, Malvern, United Kingdom) for 5 minutes, in order to break down any agglomerates present before being fed into the instrument for analysis.

A Micrometrics TriStar II BET analyzer (Micrometrics Inc., Norcross, USA) was used to obtain the Brunauer-Emmett-Teller (BET) specific surface area of the adsorbent material before and after activation. Liquid nitrogen at 77 K was used for the measurements. The samples were degassed by vacuum drying for 10 h at a temperature of 100 °C in order to remove moisture and impurities before measurement.

WAS particle morphologies were studied using an ultrahigh-resolution field emission scanning electron microscope (HR FESEM Zeiss Ultra Plus 55, Carl Zeiss AG, Oberkochen, Germany) with an InLens detector. An acceleration voltage of 1 kV was used to ensure maximum resolution of surface detail. All samples were first coated with conductive carbon using an EMITECH K950X coater. The scanning electron microscope used was also fitted with an energy dispersive X-ray spectrometer (EDS), this was used to establish the elemental composition of selected sites on the WAS particles. In order to obtain accurate results, the samples were first cast in resin, upon curing the samples were polished and carbon coated before analysis.

Fourier transform infrared (FTIR) spectra of the both raw and activated WAS before and exposure to 250 mg/L Pb(II) were recorded on a PerkinElmer Spectrum 2000GX FTIR spectrometer (Perkin

Elmer, Waltham, USA) using an attenuated total reflection (ATR) attachment. All FTIR spectra were recorded at a resolution of 1 cm^{-1} for 16 scans from 4000 to 550 cm^{-1} and represent the average of 16 scans.

X-ray photoelectron spectroscopy (XPS) was used to characterize both raw and activated WAS before and after exposure to 100 mg/L Pb(II) with a Thermo ESCAlab 250 Xi (Madison, USA). Samples were rinsed with distilled water after adsorption experiments and dried at 60 °C.

2.5. Adsorption equilibrium experiments

The equilibrium behavior of the adsorbents was studied using batch adsorption experiments. Serum bottles containing 0.5 g/L of adsorbate were prepared with 30 mL of Pb(II) solution in concentrations ranging from 0 to 1000 mg/L Pb and sealed with rubber stoppers. The bottles were agitated at 120 rpm and maintained at 30, 40 or 50 °C using a water bath (Labotec EcoBatch Model 207, Labotec (PTY) Ltd, South Africa). Due to the very heterogenous nature of WAS, equilibrium experiments were performed with sextuplicate replication. The pH as well as concentrations of lead, calcium, and zinc were measured well after equilibrium was reached (24 h) using atomic absorbance spectrophotometry (Perkin Elmer, Waltham, Massachusetts).

Isotherms were fit using least squares regression for commonly employed adsorption models. The Langmuir isotherm model is frequently used under the assumption of a fixed number of homogeneous sites where reversible, monolayer adsorption takes place with no interaction between adsorbate species [43] and can be expressed as:

$$Q_e = \frac{Q_{\max} K_L C_e}{1 + K_L C_e} \qquad 12$$

Where $Q_{\max}$ is the maximum saturated monolayer adsorption capacity (mg/g), K_L is the Langmuir adsorption equilibrium constant (L/mg) related to the affinity between adsorbate and adsorbent, and C_e is the equilibrium concentration of Pb(II) in solution (mg/L).

The Freundlich isotherm equation describes reversible, non-ideal, multilayer adsorption and is usually used for heterogeneous adsorbents like biomass [44]. This model has, however, been found to inadequately describe the linearity range at very low concentrations or saturation effects at very high concentrations [43]. The Freundlich isotherm is expressed in Equation 13 [43,44]:

$$Q_e = K_F C_e^{\alpha} = K_F C_e^{\frac{1}{n}} \quad 13$$

In Equation 13, K_F is the Freundlich constant in (mg/g)/(mg/L)$^{\alpha}$ and α is the Freundlich intensity parameter. The isotherm is linear when $\alpha = 1$, favourable when $\alpha < 1$, and unfavourable when $\alpha > 1$ [43]. In addition, it has been reported that a value for α (Equation 13) between 0 and 1 indicate the surface heterogeneity, with more heterogeneous surfaces having values closer to 0 [44].

The two-surface Langmuir model (Equation 14) was presented by Irving Langmuir in his seminal paper on adsorption modelling [45]. This model assumes that sorption takes place on two types of surfaces, each with different binding energies [45,46]. The enumeration in the subscripts indicates to which of the two surfaces the parameter belongs. This model is powerful as it provides a mechanistic description of adsorption on heterogeneous surfaces, therefore providing insights otherwise lost i.t.o. heterogeneous adsorption.

$$Q_e = \frac{Q_{\max,1} K_{L1} C_e}{1 + K_{L1} C_e} + \frac{Q_{\max,2} K_{L2} C_e}{1 + K_{L2} C_e} \quad 14$$

To ensure no precipitation of Pb, as a result of Pb hydrolysis, initial solution pH was adjusted to 4 after Hammaini, González, et al. [20] and Hawari & Mulligan [47]. Equilibrium pH, Zn(II), and Ca(II) were additionally measured. The effects of pH on adsorption capacity were determined by preparing 0.5 g/L of adsorbate with 30 mL of 100 mg/L Pb(II) solution adjusted to pH of 2, 4, and 5. pH values greater than 5 was not investigated because at pH values much greater than 4 significant Pb hydrolysis occurs with accompanying precipitation of insoluble Pb-hydroxyl complexes [48]. Additionally, the zeta potential were determined with a Malvern zetasizer Nano ZS for pH values between 2.00 and 12.00.

WAS regeneration experiments were carried out with HNO_3 [49–52] and $Ca(NO_3)_2$ [53]. Although $CaCl_2$ is generally used as a Ca(II) source for regeneration [47,51,54], it was avoided to prevent $PbCl_2$ precipitation [47]. For regeneration with HNO_3, 0.5 g/L of WAS adsorbents were exposed to 100 mg/L initial Pb(II) for 24 h. Adsorbents were thereafter recovered with filter paper and rinsed with distilled water before being dosed as 0.5 g/L into 0.1 M HNO_3 solution. Lead concentrations were measured for each step.

Regeneration with $Ca(NO_3)_2$ was studied in more detail as a preferential eluent, since acidic eluents tend to destabilize pH [47,55]. Four 24 h adsorption-desorption cycles were performed. Pb(II) was loaded in adsorption cycles using 100 mg/L $Pb(NO_3)_2$ while 1.5 M $Ca(NO_3)_2$ at pH = 4 was used to unload Pb(II) in desorption cycles. WAS was dosed at 0.5 g/L for each cycle and was recovered using filter paper. The adsorbent was also rinsed multiple times with distilled water and dried before reuse. The pH as well as concentrations of lead, calcium, and zinc were measured well after equilibrium was reached using atomic absorbance spectrophotometry.

Untreated industrial effluent was obtained from a car battery recycling plant in Germiston, South Africa. The measurement of various ions in the effluent was achieved using a 940 Professional IC Vario ion chromatograph (Metrohm, Switzerland) with separation column Metrosep C 6 – 250/4.0 (Metrohm, Switzerland) and C 6- eluent- 8 mM oxalic acid (Metrohm, Switzerland). The effluent adjusted from pH < 0.5 to pH = 4 and was dosed with 0.5 g/L and 1.0 g/L WAS for 24 h. Equilibrium Pb(II) concentration was measured using atomic absorbance spectrophotometry (Perkin Elmer, Waltham, Massachusetts). .

3. RESULTS AND DISCUSSION

3.1. Adsorption kinetics experiments

Adsorption of Pb(II) onto WAS activated by HCl and H_2SO_4 proved negligible due to the invalidation of active sites by these acids, likely as a result of hydrolysis of the carbonaceous surface by the

respective activation agent [56]. The effects of these adsorbents on solution Pb(II) concentration are presented in the supplementary material Figures S1 a) and b).

Kinetic parameters were fit to the data of Pb(II) adsorption onto raw WAS and $ZnCl_2$ activated WAS with initial concentrations of adsorbate ranging from 10 to 50 mg/L Pb(II). The parameters fit for pseudo-first-order, two-phase pseudo-first-order, and pseudo-second-order models are displayed in Table 2 and plotted in Figure 1.

In most runs, it was found that two-phase pseudo-first-order fits had the highest coefficients of determination (average $R^2 = 0.963$). This is most likely due to the separation of fast and slow adsorption rates into separate compartments, allowing for better representation of a heterogeneous surface. Additionally, the pseudo-second-order model (average $R^2 = 0.960$) was found to represent data slightly better than pseudo-first-order kinetics (average $R^2 = 0.934$). This may indicate an abundance of adsorption sites relative to Pb(II) ions in the solution [57,58].

For pseudo-first- and pseudo-second-order models, the rate constants k_1 and k_2 were found to decrease with increases in initial bulk concentration. This is due to the rate constants being inversely proportional to the time scale of the model since higher bulk concentrations of Pb(II) require longer time scales to reach adsorption equilibrium [38]. The two-phase pseudo-first-order model, however, appeared to maintain rate constants independent of initial Pb(II) concentrations but with the fraction of the fast phase decreasing with an increase in C_0. This is most likely also due to longer periods of time required for high bulk concentration adsorption to reach equilibrium, resulting in larger slow phase fractions.

Figure 1 shows how the three adsorbents have similar kinetic parameters. Raw WAS exhibits significantly faster adsorption rates than other materials, but possess lower adsorption capacities for all initial concentrations except for 50 mg/L. This is confirmed in the kinetic-model parameter estimations presented in Table 2, where on average raw WAS rate constants are the highest and adsorption capacities are the lowest across all models.

To establish the relative influence of EMT and IMT on the adsorption process, Equations 6, 7, and 10 were evaluated for the respective adsorbents (raw WAS and $ZnCl_2$ activated WAS) and the Bi numbers were estimated. The results are reported in Table 3 and the fit showing the comparison of Equation 10 with the experimental results for the respective adsorbents are shown in Figure 2. The results provide strong evidence for an IMT dominated system; $Bi \gg 100$ for all adsorbents. In addition, the IMT model (Equation 10) predicts the adsorption processes for both the WAS adsorbents very accurately. This is likely an indication that the WAS adsorption processes were dominated by IMT throughout the experimental runs, i.e. the adsorption processes were much faster than the mass transport processes.

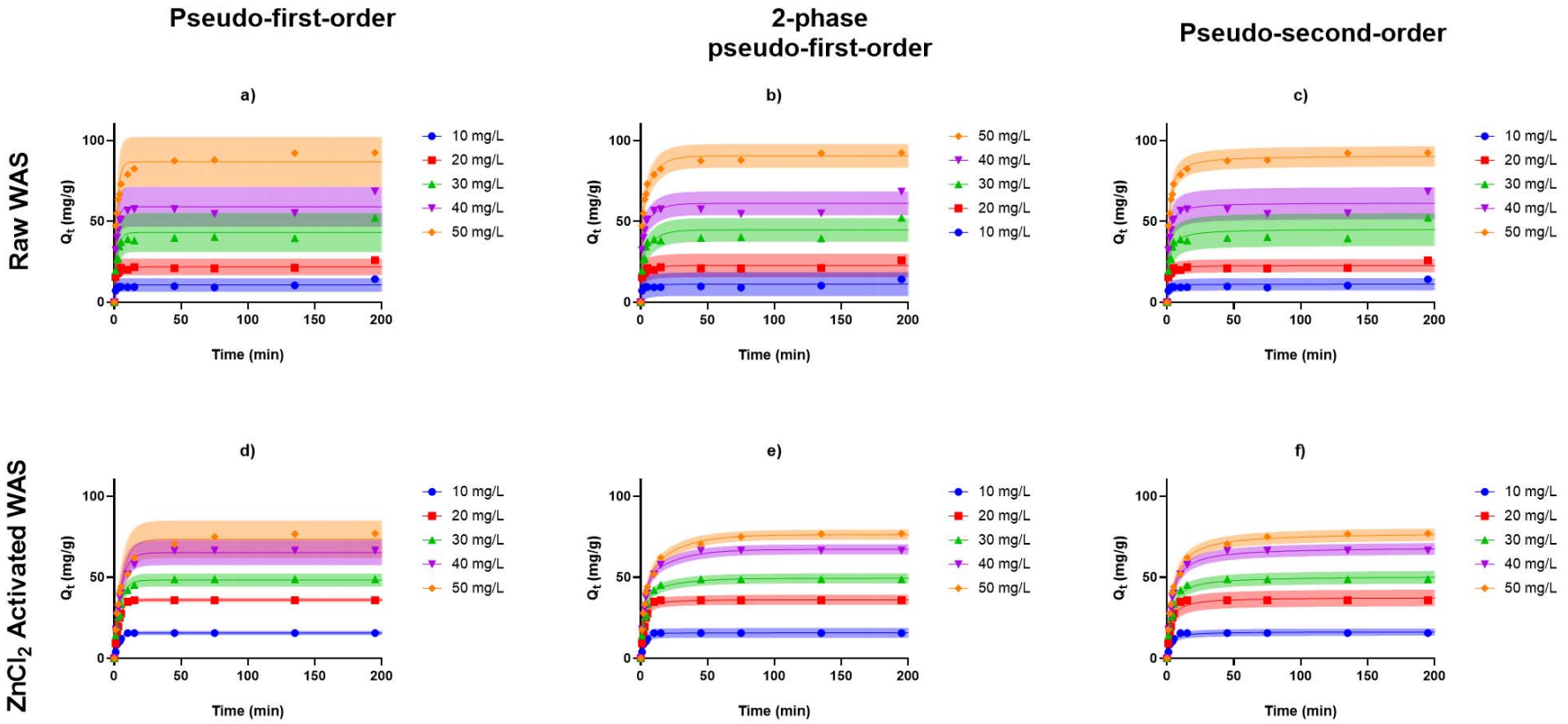

Figure 1. Adsorption rate curve of Pb(II) onto raw and activated WAS shown with 95 % prediction intervals shown as shaded areas. a-c: Raw WAS, d-f: $ZnCl_2$ activated WAS, for initial Pb(II) concentrations ranging from 10 mg/L to 50 mg/L. The 95% prediction interval indicates the region within which there is a 95% probability of future observation [59,60].

Table 2. Kinetic parameters for the adsorption of varied concentrations of Pb(II) solution onto unactivated WAS, $ZnCl_2$ activated WAS.

Adsorbent	C_0 (mg/L Pb)	Pseudo-first-order			Two-phase pseudo-first-order					Pseudo-second-order		
		Q_e (mg/g)	k_1 (1/min)	R^2	$Q_{e,fast}$ (mg/g)	$Q_{e,slow}$ (mg/g)	$k_{1,\text{fast}}$ (1/min)	$k_{1,\text{slow}}$ (1/min)	R^2	Q_e (mg/g)	k_2 (g/[mg·min])	R^2
Raw WAS	10	10.7	0.901	0.750	8.54	2.76	1.34	0.117	0.797	11.2	0.131	0.799
	20	21.8	0.956	0.894	18.31	4.49	1.34	0.117	0.929	22.8	0.0783	0.935
	30	43.0	0.423	0.876	24.63	20.07	1.34	0.117	0.900	45.3	0.0148	0.913
	40	59.0	0.560	0.921	40.88	20.32	1.34	0.117	0.943	61.5	0.0162	0.950
	50	86.8	0.483	0.942	54.42	35.98	1.34	0.117	0.992	90.7	0.00919	0.991
$ZnCl_2$ activated WAS	10	15.7	0.324	0.991	15.28	0.42	0.344	0.0444	0.990	16.4	0.317	0.970
	20	36.0	0.288	0.998	33.07	3.03	0.344	0.0444	0.994	37.6	0.180	0.972
	30	48.2	0.239	0.993	38.36	10.94	0.344	0.0444	0.993	50.6	0.00713	0.991
	40	65.1	0.208	0.986	46.30	20.90	0.344	0.0444	0.995	68.5	0.00446	0.996
	50	73.4	0.182	0.975	46.56	29.64	0.344	0.0444	0.997	77.7	0.00333	0.997

Table 3. Parameters fit for the determination of EMT and IMT influences in the adsorption of Pb(II) onto WAS.

	k_f(m.s^{-1})	Adjusted R^2	D_e (m^2.s^{-1})	Adjusted R^2	Bi
Raw WAS	3.15×10^{-4}	0.8557	3.71×10^{-12}	0.9363	17466
$ZnCl_2$ Activated WAS	4.61×10^{-4}	0.9127	1.75×10^{-12}	0.9623	54304

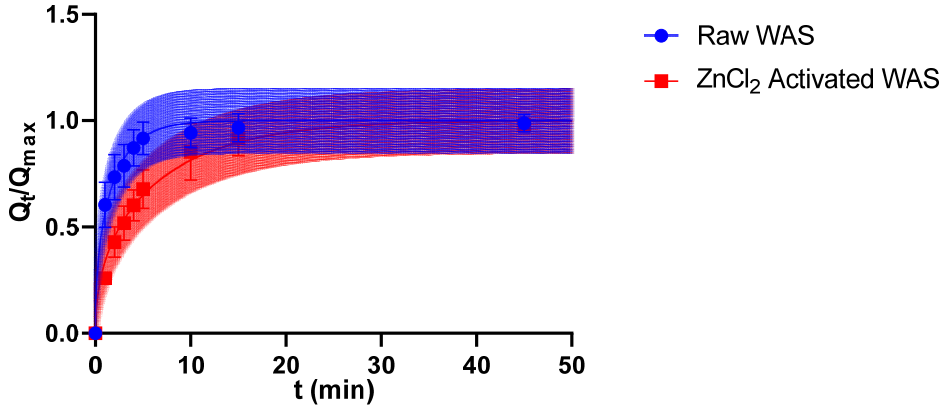

Figure 2. Fitted experimental adsorption kinetics relative to maximum adsorption using the Crank diffusion model shown with a 95 % prediction interval in the shaded area.

3.2. Characterization of adsorbents

3.2.1. Particle size distribution and BET surface area

The particle characteristics of the WAS before and after $ZnCl_2$ activation is presented in Table 4 below**.** The median particle size (d_{50}) of both samples was large with 206 and 187 µm recorded for raw and activated WAS, respectively. The smaller particle size for activated WAS is likely a result of the grinding down with a mortar and pestle after drying the sample. The BET surface area of the two samples is also recorded in Table 4. An 83.5% increase in surface area was observed in the $ZnCl_2$ activated WAS (1.78 m^2/g) compared to the initial material (0.97 m^2/g). This observation is consistent with findings from other researchers who also reported increased surface areas when using $ZnCl_2$ as an activating agent [61]. It should be noted that, assuming spherical sludge particles with an average diameter equivalent to the d_{50} diameters shown in Table 4 and an average sludge density of 1.24 g/mL

[62], specific external surface areas of 0.023 m^2/g and 0.026 m^2/g for the raw WAS and $ZnCl_2$ activate WAS particles can be calculated, respectively. This indicates that as much as 98% to 99% of the total raw WAS and $ZnCl_2$ activate WAS surfaces areas consisted of intraparticle surface areas and therefore most adsorption sites were intraparticle. This supports the observation that intraparticle diffusion was the rate limiting step in the system (Figure 2 and Table 3).

Table 4. Volume-based particle size distribution and BET surface areas of the WAS before and after $ZnCl_2$ activation raw materials used.

	d_{10}[a] (μm)	d_{50}[a] (μm)	d_{90}[a] (μm)	BET surface area (m^2/g)
Raw WAS	17.4	206	449	0.97
$ZnCl_2$ Activated WAS	53.3	187	396	1.78

[a] d_i refers to the diameter which a certain percentage (i %) of particles are smaller than.

3.2.2. Particle morphology and EDS

Figure 3 presents a FESEM micrograph of the WAS before and after activation. In both cases, the particles exhibited irregular particle morphology. Despite the vigorous pre-treatment grinding process, it was evident that the particles were highly agglomerated. The activated WAS exhibited agglomeration of an order of magnitude bigger than the raw WAS. Another peculiar observation was the presence of rod-like particles in the activated WAS which did not appear in the raw WAS images. The reason for their occurrence is not known at present. The EDS spectra results obtained for the WAS samples in conjunction with the FESEM micrographs can be observed in **Figure 3**. The $ZnCl_2$ activated WAS showed the presence of Zn which was absent in the raw sample.

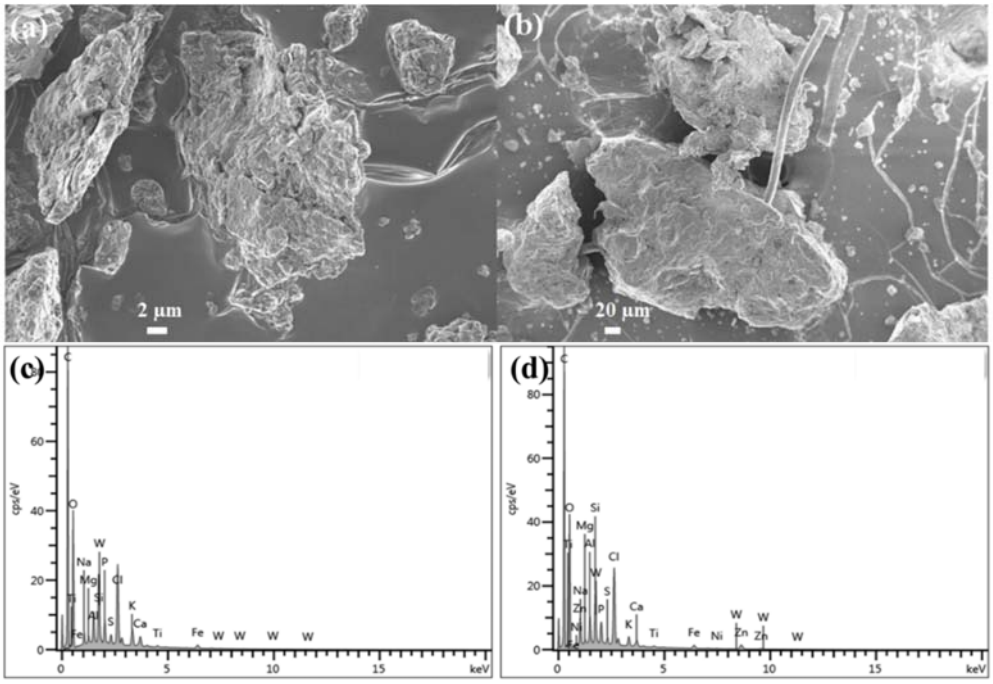

Figure 3. FESEM micrograph of the WAS (a) before and (b) after activation; (c) and (d) show the corresponding EDS spectra of the WAS before and after $ZnCl_2$ activation, respectively.

3.2.3. FTIR

Fourier transform infrared spectroscopy was used to investigate the functional groups present in the WAS adsorbent material. FTIR spectra of between 4000 and 550 cm^{-1} wavenumbers were recorded. Both adsorbents had similar functional group bands which suggest that the $ZnCl_2$ activation did not greatly influence the surface chemistry. The spectra in Figure 4 presented great similarity to results recorded in literature for sewage sludge [63–66]. A broad peak recorded in the range 3600 to 3000 cm^{-1} was attributed to variable stretching of O-H involved in variegated hydrogen bonding, which is normally present in acids and alcohols. Vibrational peaks observed between wavenumbers 2980 and 2800 cm^{-1} were attributed to C–H stretching, which is associated with the presence of aliphatic chains [65]. The band at 2924 cm^{-1} is representative of the asymmetrical C–H stretching in the methyl group while the band at 2854 cm^{-1} was likely due to the symmetrical stretching of the C–H bonds from the methylene groups [67].

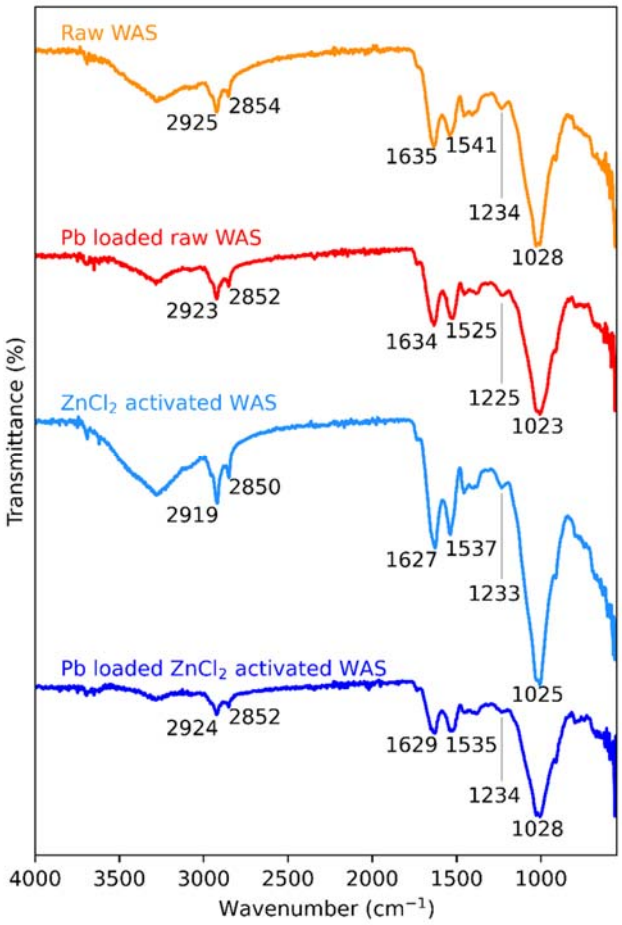

Figure 4. FTIR spectra of WAS adsorbents before and after Pb(II) adsorption.

The bands close to 1455 and 730 cm^{-1} were due to CH_2 scissoring and rocking vibrations, respectively. The presence of -C=O bonds from amide I was signaled by bands around 1630 cm^{-1} while C-N stretching from amide II was highlighted by the bands around 1540 cm^{-1} [63]. Bands at 1407 and 1230 cm^{-1} were assigned to the symmetric stretching of carboxylate groups and C–O stretching in carboxylic acids, respectively. The prominent band between 1170 and 1000 cm^{-1} is attributed Si-O-Si asymmetrical stretching characteristic of WAS [63,66,68]. The wide range of polar functional groups present on the activated WAS highlight the usefulness of the material as an effective adsorbent due to the possible electrostatic interactions between the Pb and the surface groups.

Significant peak shifts are seen following WAS activation with $ZnCl_2$. The amide I peak shifted from 1635 to 1627 cm^{-1} while amide II shifted from 1541 to 1537 cm^{-1}. This may be indicative of Zn binding affecting oscillations in amide functional groups.

The loading of Pb(II) onto adsorbents affected C-N and C-O stretching in raw WAS, as seen in the shifting of peaks from 1541 to 1525 and 1234 to 1225 cm^{-1} respectively. This suggests the involvement of amide and carboxyl groups in adsorption. Interestingly, supplementary Figure S2 illustrates the complete disappearance of bands for C-O, C-N, and O-H stretching in HCl and H_2SO_4 activated WAS. It is likely that this disappearance was a significant contributing factor for poor adsorption capacity in these adsorbents. Little to no shift is seen for C-N and C-O stretching in $ZnCl_2$ activated WAS (1537 to 1535 cm^{-1} and 1233 to 1234 cm^{-1}), possibly due to these functional groups not significantly being involved in adsorption. The red shift of the Si-O-Si peak (5 cm^{-1}) in raw WAS may be a result of Pb adsorption. A decrease in wavenumber decrease has been reported for increased metal/silicon ratio [69], but the small magnitude of the shift and lack of reflected behavior in $ZnCl_2$ activated WAS may highlight the in significance of this observation.

3.2.4. XPS Analysis

Figure 5a) shows the wide scan XPS spectra of the WAS adsorbents before and after adsorption of Pb(II). The disappearance of the Ca2p3/2 peak from WAS at 347.1 eV is noticeable following $ZnCl_2$ activation. The presence of Zn following $ZnCl_2$ activation was signaled by the peaks at 1045.2 and 1022.3 eV, corresponding to Zn2p1/2 and Zn2p3/2 respectively and indicates the presence of ZnO (Figure 5b)). The 22.9 eV difference between the two peaks is characteristic of Zn(II) [70]. The decrease in Zn2p peak intensity also suggests the removal of Zn(II) ions following lead adsorption. Adsorbed lead is indicated by peaks at ~414 and ~437 eV corresponding to Pb4d [71], as well as peaks at 138.5 and 143.2 eV corresponding to Pb4f7/2 and Pb4f5/2 respectively (Figure 5c)) [72].

Figure 5d) shows the Si2p peaks for all adsorbents at 102.2 eV with the exception of raw WAS at 102.0 eV [73]. N1s peaks were observed between 399.5 and 399.8 eV for raw WAS, Pb-loaded raw

WAS, $ZnCl_2$ activated WAS, and Pb-loaded $ZnCl_2$ activated WAS (Figure 5e)), characteristic of amide functional groups – as observed in the FTIR analyses [74].

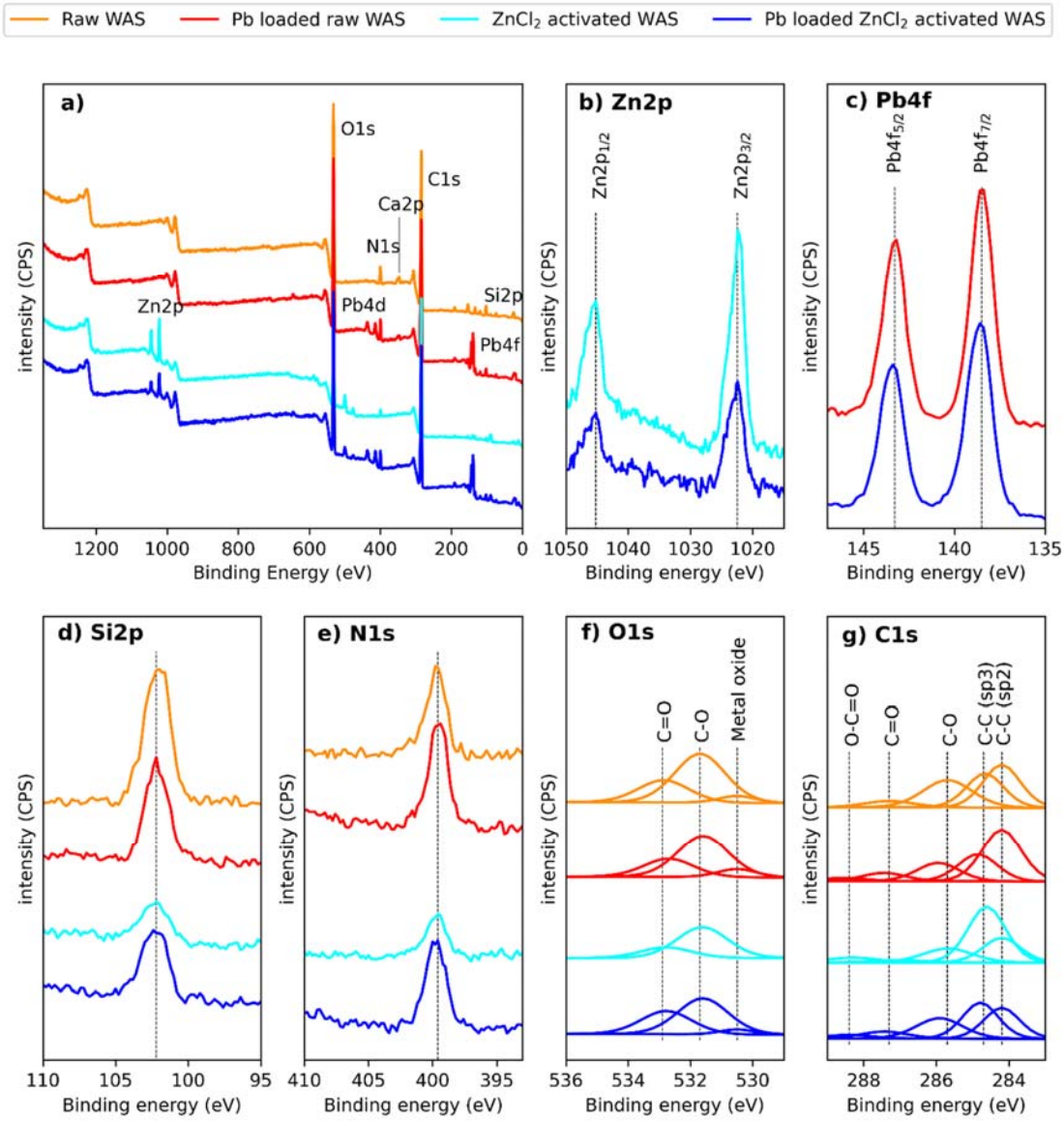

Figure 5: XPS spectra of WAS adsorbents before and after adsorption: a) wide-scan spectra, b) high resolution Zn2p spectra, c) high resolution Pb4f spectra, d) high resolution Si2p spectra, e) high resolution N1s spectra, f) high resolution O1s spectra, and g) high resolution C1s spectra.

Deconvoluted O1s peaks are shown in Figure 5g). Metal oxide, C-O and C=O exhibited peaks respectively at 530.5, 531.7, and 532.9 eV for raw WAS; 530.5, 531.6, and 532.7 eV for Pb-loaded

raw WAS; no peak observed, 531.6, and 532.8 eV for $ZnCl_2$ activated WAS; 530.5, 531.6, and 532.8 eV for Pb loaded $ZnCl_2$ activated WAS. The absence of an increase in binding energy of O1s and N1s peaks, usually associated with heavy metal-oxygen coordination [75–77], provides evidence for the presence of pure ion exchange which depend entirely on coulombic attraction [78].

Figure 5f) shows the C1s scan. The heterogeneity of WAS is highlighted here, as the significant variety in C-C sp3 and C-C sp2 can be attributed to diverse organic compounds rather than changes in chemical structure brought about by $ZnCl_2$ or $Pb(NO_3)_2$.

3.2.5. Influence of particle characteristics on adsorption kinetics

Considering the characterization results, it is interesting to note the similarity in the observed adsorption behavior between the raw WAS and activated WAS (Figure 1). It is clear from the BET, particle size results, and FESEM that the adsorption behavior is a result of more intricate surface properties of the adsorbent as opposed to merely the physical surface properties such as specific surface areas and morphology. The slower kinetic rates observed in $ZnCl_2$ activated WAS in **Figure 1** and **Table 2** may be attributed to the particle agglomeration observed in Figure 3.

The similarities in the surface species present the adsorbents tested, with slight variation in the resolution of the band, provide some insight into the similarities in the adsorption behavior observed.

3.3. Adsorption equilibrium experiments

The lack of Pb(II) adsorption from HCl and H_2SO_4 activated WAS during kinetic studies prompted no further investigations into the adsorption equilibria of these materials.

A paired t-test determined that Pb(II) adsorption differed significantly between $ZnCl_2$ activated WAS and raw WAS ($p = 0.0252$).

Additionally, a two-way ANOVA assessing the role of temperature and initial concentration on adsorption determined that the 20 °C temperature range over which the experiments were performed

did not have a significant effect on the adsorption capacity of both raw and $ZnCl_2$ activated WAS (p = 0.134). As a result, no meaningful thermodynamic analysis could be done.

3.3.1. Adsorption isotherm models

The lack of influence of temperature on adsorption capacity resulted in global isotherms being fit for adsorption data across all temperatures. Parameters obtained from the fitting of various isotherm models are presented in Table 5, and this data is visualized in Figure 6. The value of R^2 was calculated for each of the models and was found to have decreasing magnitudes in order: Two-surface Langmuir > Freundlich > Langmuir. The lowest coefficients of determination overall for the Langmuir adsorption isotherms is likely due to the assumption of homogeneous adsorption sites misrepresenting the wide range of sites involved in adsorption that were identified during WAS characterization. The Freundlich adsorption isotherm accounting for surface heterogeneity exhibited the second-best fit. This goodness of fit may in addition suggest multilayer adsorption on the surface of the WAS [79,80]. Two-surface Langmuir adsorption isotherms appear to fit best. This is most likely due to the grouping of the diverse adsorption sites into different binding sites which allow for a comparatively better description of adsorption. The types of binding sites are seen in the differences between the two-surface Langmuir equilibrium constant values (K_{L1} and K_{L2}), where K_{L1} tends to infinity, therefore indicating effectively irreversible adsorption, while the values for K_{L2} were all less than 1.0×10^{-2} L.mg^{-1} – indicating significantly reversible adsorption. The irreversibility in adsorption is seen in the sudden drop in the Q_e values as C_e tends to 0 (Figure 5), therefore validating the two surface Langmuir isotherm model for adsorption.

Table 5. Adsorption data of Pb(II) onto raw and $ZnCl_2$ activated WAS fit to isotherm models.

		Langmuir		**Freundlich**		
Adsorbent	Q_{max}	K_L (L. mg^{-1})	R^2	K_F (mg/g)/(mg/L)$^{\alpha}$	α	R^2
Raw WAS	307	0.00535	0.906	19.8	2.61	0.910
$ZnCl_2$ activated WAS	274	0.00554	0.778	39.7	3.89	0.851
		Two-surface Langmuir				
Adsorbent	$Q_{max,\,1}$ (mg.L^{-1})	K_{L1} (L. mg^{-1})	$Q_{max,\,2}$ (mg.L^{-1})	K_{L2} (L. mg^{-1})	R^2	
Raw WAS	331	1.80×10^{12}	32.1	0.00348	0.919	
$ZnCl_2$ activated WAS	348	5.04×10^{19}	66.9	0.00171	0.869	

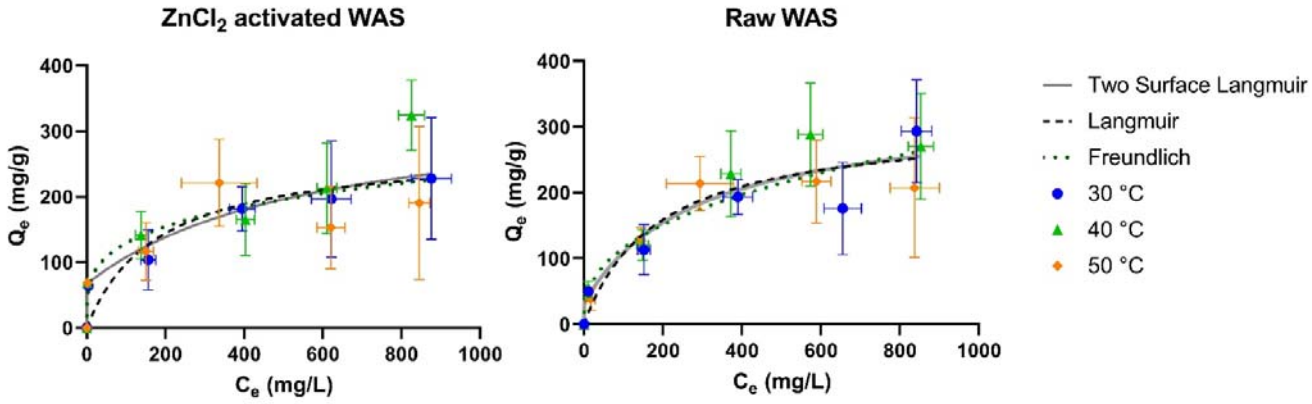

Figure 6: Temperature independent adsorption isotherms for $ZnCl_2$ activated and raw WAS. The error bars represent the standard deviations of the sextuplicate equilibrium experiments.

3.3.2. Adsorption mechanism

Adsorption onto biomass has been attributed to a combination of multiple mechanisms [17,81,82]. Figure 7 suggests dual mechanisms of cation exchange and electrostatic attraction [83]. This is seen with cations that were released into solution as Pb was adsorbed (ion exchange). Above certain Pb(II) adsorption amounts, however, there is no observable influence of Pb(II) adsorption on cation concentration in solution (electrostatic attraction). Piecewise linear functions have been fit in Figure 7 to assist in distinguishing the mechanisms.

For both WAS adsorbents, control runs ($C_0 = 0$) resulted in increases in equilibrium pH from the initial pH of 4. This indicates the adsorption of hydrogen ions onto binding sites. Figure 7**Error! Reference source not found.**a) illustrates the effect of lead adsorption on equilibrium pH for both WAS adsorbents. The decrease in proton adsorption (and eventual proton release) with increased Pb(II) adsorption demonstrates binding site competition between the H^+ and Pb^{2+} ions. $ZnCl_2$ activated WAS demonstrated a greater affinity for proton adsorption than raw WAS, possibly contributing to the slightly lower Pb(II) adsorption capacity. The release of Ca(II) and Zn(II) into solution following Pb(II) adsorption is shown in Figure 7b) and Figure 7c) respectively, with both ions increasing in equilibrium concentration following increases in Pb(II) adsorption. These results are characteristic of a cation exchange mechanism [84]. Lower Ca(II) concentrations in $ZnCl_2$ activated WAS adsorption effluent is supported by the loss of surface calcium observed in XPS analysis (Figure 5a)). The removal of calcium likely happened as an exchange between Zn(II) and Ca(II) during chemical activation, as zinc selectivity over calcium is reported in several ion exchange materials [85–88]. The greater selectivity of Pb(II) or Zn(II) over protons arises from higher ion charge [84,89,90]. The selectivity sequence among divalent cations Pb(II) > Zn(II) arises from smaller hydration radii being favored for binding [84,89–91], with a radius of 0.405 and 0.430 nm for Pb(II) and Zn(II) respectively [92].

Stoichiometrically an ion-exchange mechanism can be represented by equation 16 [84]

$$M^{\alpha+}\left(X^{\beta-}\right)_{\frac{\alpha}{\beta}} + \frac{\alpha}{\gamma}N^{\gamma+} \rightarrow \frac{\alpha}{\gamma}N^{\gamma+}\left(X^{\beta-}\right)_{\frac{\alpha}{\gamma}} + M^{\alpha+} \qquad 15$$

With α, β and γ the respective valence absolute values of M, X, and N respectively.

In the specific case at hand the ion exchange mechanism yields increasing amounts of H^+, Zn^{2+} and Ca^{2+} ions to the solution dependent on the prevalence in the adsorbent and the amount of Pb adsorbed. Figure 7 clearly show that the greater the amount of Pb^{2+} adsorbed, the greater the amount of Zn^{2+}, Ca^{2+} released to the solution. Additionally, competition between H^+ and Pb^{2+} result in a net increase in H^+ ions in solution, consequently validating the proposed ion exchange mechanism. Furthermore,

the absence of significant shifts in the N1s and O1s binding energies observed in the XPS results (Figure 5) indicates the prevalence of pure electrostatic ion exchange [78].

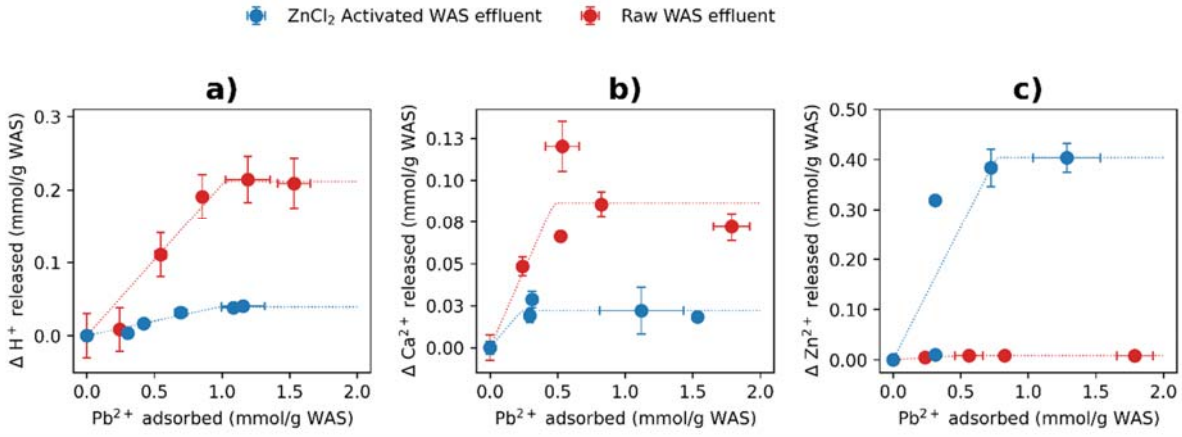

Figure 7: Difference in solution cation concentrations between lead-free control and lead-loaded solution, with a) H^+, b) Ca^{2+}, and c) Zn^{2+} released vs. the Pb^{2+} adsorbed. Error bars show standard error.

According to Kumar and Jain [84], ion exchange rates are dominated by diffusional limitations, therefore validating the observation that severe mass transfer limitations were present in the system for both adsorbent types.

3.3.3. Effect of pH

In comparison to a pH of 4, using an initial pH of 2 caused the equilibrium adsorption capacity of $ZnCl_2$ activated WAS as well as the raw WAS dropped to effectively negligible levels (See supplementary figure S3). This significant reduction in adsorption capacity with lower pH demonstrates competition between H^+ and Pb(II) ions and supports the proposed mechanism of cationic ion exchange. For pH values much greater than 4 significant Pb hydrolysis occurs with the accompanying precipitation of insoluble Pb-hydroxyl complexes [48]. For a pH increase from 4 of 5, a statistically insignificant difference in Pb(II) removal was observed for the raw WAS ($p = 0.482$) and $ZnCl_2$ activated WAS ($p = 0.641$), respectively (Figure S3).

Figure 8 shows how both adsorbents have negative zeta potentials above a pH 4, resulting in enhanced adsorption due to the positive charge of the adsorbate [93]. The pH at points of zero charge (pH_{PZC}) were determined as 2.58 and 2.30 for $ZnCl_2$ activated WAS and raw WAS respectively, and are similar to values reported for secondary sludge and organic materials [94,95]. The higher zeta potential measurements and pH_{PZC} for $ZnCl_2$ activated WAS is likely due to the reduction of available negatively charged functional groups, resulting in a reduction of the negative surface charge [82].

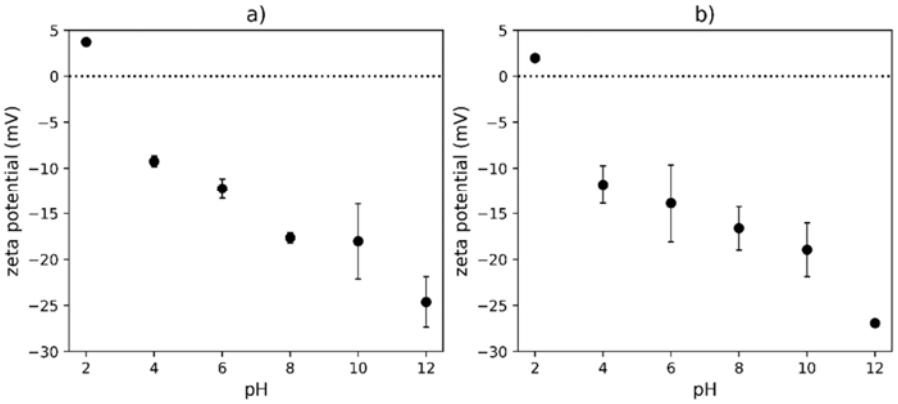

Figure 8: Effect of pH on the zeta potential of a) $ZnCl_2$ activated WAS and b) raw WAS. Error bars show standard error.

3.3.4. Regeneration

Adsorbent regenerated using HNO_3 showed circa 32 % and 38 % drop in adsorption capacity with effectively complete recovery of Pb(II) for raw and $ZnCl_2$ activated WAS, respectively.

Results from regeneration with $Ca(NO_3)_2$ are illustrated in Figure 9. Figure 9a) shows a 44 % loss in adsorption capacity after the first adsorption cycle for raw WAS, subsequently the adsorption capacity was maintained through to the fourth cycle. Interestingly, the second $ZnCl_2$ activated WAS adsorption cycle showed a slight increase in adsorption capacity (8.01 %) from the first cycle. This was likely due to Ca-Zn ion exchange (Figure 9c) in the first desorption cycle that allowed for greater Pb-Ca ion exchange in the second adsorption cycle. The fourth cycle saw the adsorption capacity of

$ZnCl_2$ activated WAS as 24.5 % less than the first cycle. Nearly constant specific desorption capacities of Pb(II) from both adsorbents (approximately 0.2 mmol/g WAS) across all four cycles were observed – consistent with observations by Lalmi et al. [53] who observed nearly constant exchange of Pb(II) by Ca(II) (from $Ca(NO_3)$) for eight consecutive elution cycles. Figure 9c) and Figure 9d) illustrate the diminished role of Zn(II) ion exchange as a Pb(II) removal mechanism as Zn(II) was removed with each cycle.

Proton adsorption appeared to decrease with each cycle, possibly due the exhaustion of binding sites. By the fourth adsorption cycle, proton adsorption was low enough for the protons released during lead-hydrogen ion exchange to decrease solution pH [47].

The ratio of Ca(II) desorption over Pb(II) adsorption indicated a significant increase in the role of Ca-Pb ion exchange during Pb(II) removal. The first adsorption cycle saw a ratio of 0.332 for raw WAS and 0.156 for $ZnCl_2$ activated WAS. By the fourth adsorption cycle, the ratios were 1.01 for raw WAS and 0.727 for $ZnCl_2$ activated WAS. The large amount of Ca(II) released during the second adsorption cycle was significantly greater than the Pb(II) removed, and it is likely from superficially bonded calcium in addition to calcium released from ion exchange.

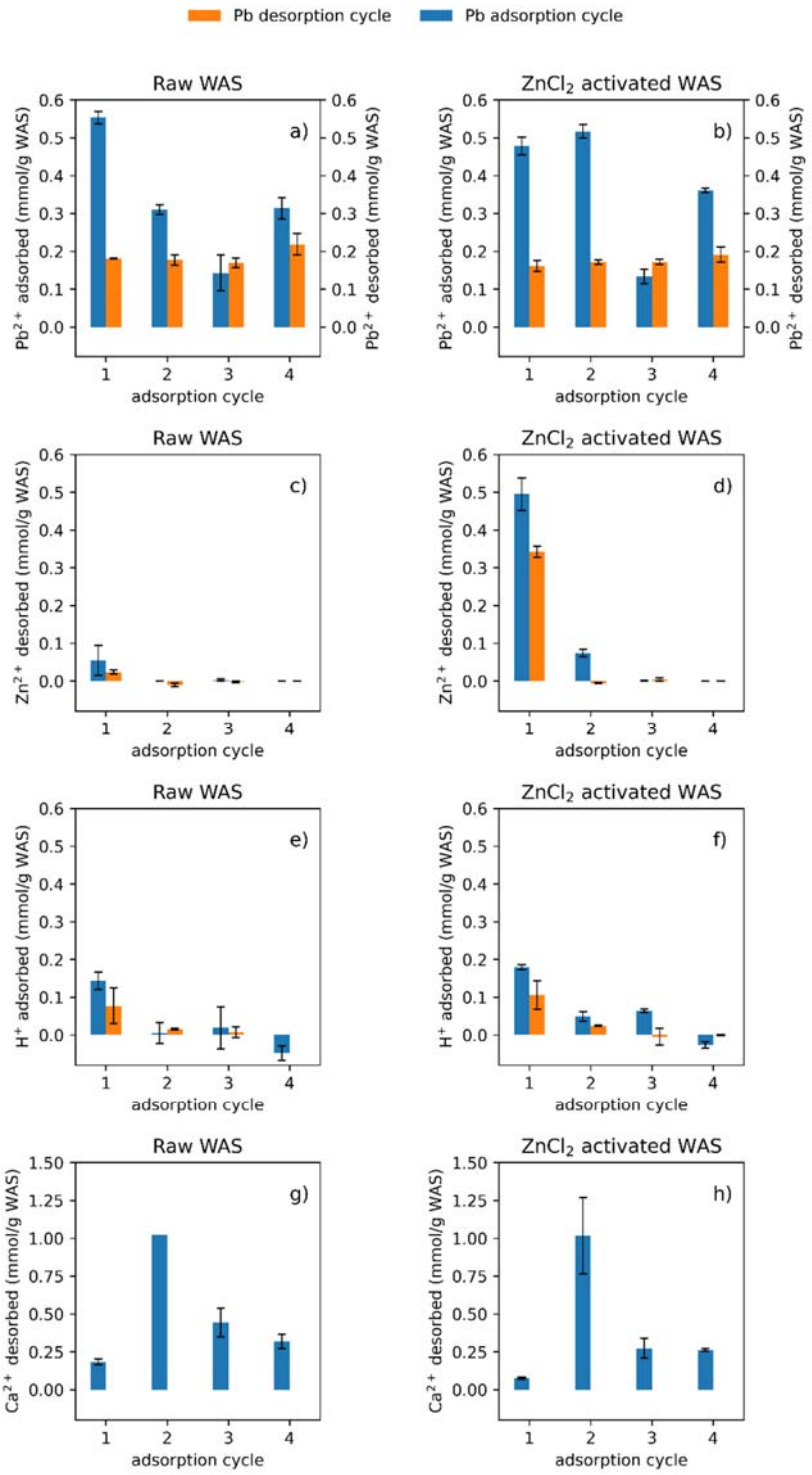

Figure 9: Cations adsorbed from or released into solution after adsorption/desorption cycles. Error bars represent standard error. Changes in Ca^{2+} concentration are not shown for the elution step in g) and h) since, after dilution for measurement, Ca^{2+} concentration variations are within one standard deviation of AA measurements.

3.3.5. Application of adsorbents to authentic industrial effluent

Table 6: Composition of industrial effluent

Ion	mg/L
Pb^{2+}	6.31
NO_2^-	0.044
Br^-	0.064
SO_4^{2-}	0.677
Li^+	0.015
Na^+	38.69
NH_4^+	0.015
K^+	0.029
Ca^{2+}	0.118

The concentration of various ions in solution for untreated battery recycling plant effluent is given in Table 6. The industrial effluent Pb(II) removal efficiency by the two different adsorbent concentrations (0.5 g/L and 1.0 g/L) are shown in Figure 10 and indicates that both adsorbents are capable of significant removal of Pb(II) from industrial effluent. The relatively lower adsorption of Pb(II) by the raw WAS as compared to the $ZnCl_2$ activated WAS was potentially a result of competition from other ions in solution (see Table 6).

To assess the comparison of the results shown in Figure 10 with the results obtained from simulated Pb(II) solutions, the industrial effluent Pb(II) adsorption results were compare to Pb(II) removal predicted using parameters fit to the Langmuir isotherm model (Equation 12 and Table 5). This comparison is shown in Figure 11; Equation 12 under-predicted the $ZnCl_2$ activated WAS results while over-predicting the raw WAS. However, considering the significant variation in equilibrium Pb(II) adsorption results (Figure 6) as a result of the heterogeneity of the adsorbents, the model predictions in this case fall well within the prediction range for the model demonstrating that Pb(II) adsorption from the

industrial effluent compares well to simulated Pb(II) solutions for both adsorbents. In addition, this means that the adsorbents performed as expected for the industrial effluent and consequently no convincing conclusions around the mechanism for the apparent reduction in adsorption for the raw WAS as compared to the $ZnCl_2$ activated WAS can be drawn.

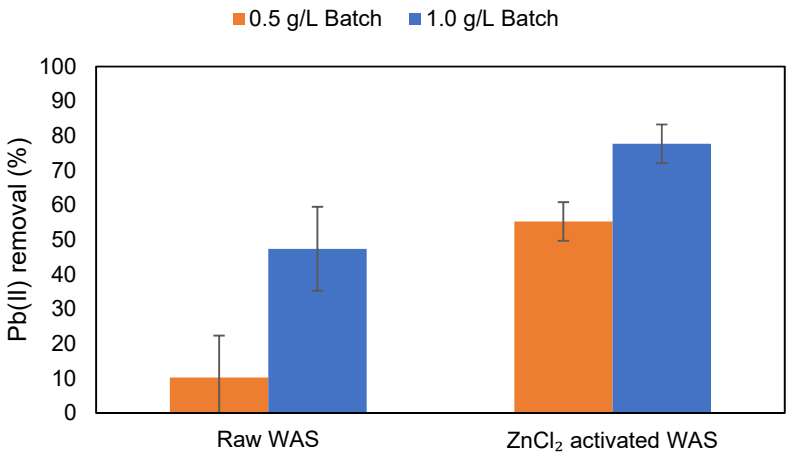

Figure 10: Percentage Pb(II) removal of WAS suspended in industrial effluent. Error bars represent the standard error of the measurements.

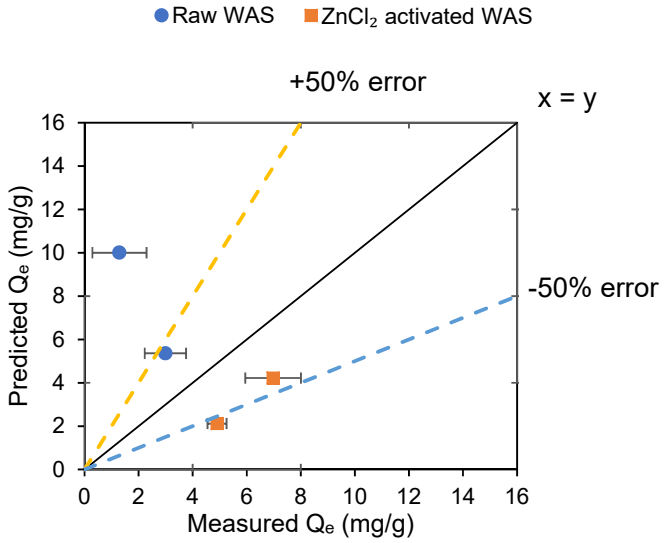

Figure 11: Parity plot showing experimental vs predicted WAS adsorption in capacity for industrial effluent. The ±50% error lines represent a 50% deviation from the predicted Q_e value. The error bars represent the standard errors of the measurements.

3.3.6. Comparison of adsorption capacity with previous studies

The maximum adsorption capacities of several sludge-based adsorbents are presented in Table 7 for comparison. It is evident that raw WAS has a comparatively high adsorption capacity without additional chemical or pyrolitic activation processes. This characteristic, coupled with the relative abundance of WAS and low cost of material preparation, make it a favorable material for the removal of Pb(II) from industrial wastewater.

Table 7. Langmuir adsorption capacity for Pb(II) on sewage sludge-based adsorbents from previous studies.

Adsorbent description	Q_{max} (mg/g)	Reference
Raw WAS	307	This study
Municipal sludge-derived biochar	289	Wang, Guo, et al. [21]
$ZnCl_2$ activated WAS	274	This study
$ZnCl_2$ activated magnetic sewage sludge biochar	249	Ifthikar, Wang, et al. [27]
Electromagnetic pyrolized biochar	198	Xue, Wang, et al. [22]
Raw WAS	143	Hammaini, González, et al. [20]
Amino-functionalized magnetic aerobic granular sludge- biochar	127	Huang et al. [28]
Magnetic sewage sludge biochar	99.9	Ifthikar, Wang, et al. [27]
Pyrolusite-modified sewage sludge carbon	69.9	Fan, Chen, et al. [29]
Pyrolusite loaded sewage sludge-based activated carbon	66.1	Xie, Jiang, et al. [30]
$ZnCl_2$ activated, pyrolyzed sewage sludge	64.1	Rozada, Otero, et al. [24]
KOH activated sludge-based biochar	57.5	Zhang, Shao, et al. [26]
Sludge derived biochar	50.0	Li, Yao, et al. [96]
Humic acid-enhanced sludge derived biochar	48.3	Zhou, Wang, et al. [23]
Potassium acetate activated sludge-based biochar	47.6	Zhang, Shao, et al. [26]

Iron oxide modified sewage sludge	42.4	Phuengprasop, Sittiwong, et al. [31]
Sludge derived biochar	40.8	Zhou, Wang, et al. [23]
Pyrolyzed sewage sludge	40.3	Rozada, Otero, et al. [24]
CO_2 activated sludge-based biochar	22.4	Zhang, Shao, et al. [26]
Sludge derived biochar	18.2	Zhang, Mao, et al., [25]

4. CONCLUSIONS

Raw waste activated sludge was found to be a fast and highly effective Pb(II) adsorbent, with a Langmuir adsorption capacity of 307 mg/g, BET surface area of 0.97 m^2/g, and pH_{PZC} of 2.30 measured. A significant effect of pH was observed with nearly negligible adsorption at pH 2 and an insignificant increase in adsorption at pH > 4; adsorption was unaffected by temperatures between 25-45 °C. The use of the chemical activation reagents $ZnCl_2$, HCl and H_2SO_4 showed no clear advantages in adsorption capacity or kinetics. The Pb(II) adsorption process in raw and $ZnCl_2$ activated WAS was dominated by IMT. Adsorption occurs as cationic exchange between H^+, Zn^{2+}, Ca^{2+} and Pb^{2+} at low lead adsorption, followed by electrostatic attraction as more lead is adsorbed. $Ca(NO_3)_2$ and HNO_3 were both demonstrated as effective eluents. Both the raw WAS and $ZnCl_2$ activated WAS showed significant Pb(II) removal from authentic Pb(II) containing industrial effluent, with the removal capacities comparing well with simulated Pb(II) model predictions. Both comparisons with modified and unmodified sludges from literature highlight raw WAS as an attractive Pb(II) adsorbent that does not require intensive processing.

5. CRediT AUTHOR STATEMENT

B. van Veenhuyzen: Methodology, Validation, Formal analysis, Investigation, Writing - Original Draft, Review & Editing, S.T. Tichapondwa: Formal analysis, Investigation, Writing - Original Draft, C. Hörstmann: Methodology, Formal analysis, Investigation, Supervision, E.M.N. Chirwa: Writing -

Review & Editing, Project administration, Supervision, H. G. Brink: Conceptualization, Methodology, Data Curation, Writing - Review & Editing, Visualization, Resources, Project Administration, Supervision

6. ACKNOWLEDGMENT

This work is based on the research supported in part by the National Research Foundation of South Africa (Grant Numbers 106938 and 121891).

7. AUTHOR INFORMATION

Corresponding author

H. G. Brink - Department of Chemical Engineering, Faculty of Engineering, Built Environment and Information Technology, University of Pretoria, Pretoria, South Africa; https://orcid.org/0000-0002-4699-6152; Phone: +27842068338; Email: deon.brink@up.ac.za

Authors

B. van Veenhuyzen - Department of Chemical Engineering, Faculty of Engineering, Built Environment and Information Technology, University of Pretoria, Pretoria, South Africa; https://orcid.org/0000-0002-5179-2736

S. Tichapondwa Department of Chemical Engineering, Faculty of Engineering, Built Environment and Information Technology, University of Pretoria, Pretoria, South Africa; https://orcid.org/0000-0003-3773-4131

C. Hörstmann - Department of Chemical Engineering, Faculty of Engineering, Built Environment and Information Technology, University of Pretoria, Pretoria, South Africa; https://orcid.org/0000-0001-9850-2313

E. Chirwa - Department of Chemical Engineering, Faculty of Engineering, Built Environment and Information Technology, University of Pretoria, Pretoria, South Africa; https://orcid.org/0000-0002-6255-862X

8. REFERENCES

[1] M.M. Naik, S.K. Dubey, Lead resistant bacteria: Lead resistance mechanisms, their applications in lead bioremediation and biomonitoring, Ecotoxicol. Environ. Saf. 98 (2013) 1–7. https://doi.org/10.1016/j.ecoenv.2013.09.039.

[2] J. Wang, C. Chen, Biosorbents for heavy metals removal and their future, Biotechnol. Adv. 27 (2009) 195–226. https://doi.org/10.1016/j.biotechadv.2008.11.002.

[3] F. Fu, Q. Wang, Removal of heavy metal ions from wastewaters: A review, J. Environ. Manage. 92 (2011) 407–418. https://doi.org/10.1016/j.jenvman.2010.11.011.

[4] S. Tunali, A. Çabuk, T. Akar, Removal of lead and copper ions from aqueous solutions by bacterial strain isolated from soil, Chem. Eng. J. 115 (2006) 203–211. https://doi.org/10.1016/j.cej.2005.09.023.

[5] N.K. Soliman, A.F. Moustafa, Industrial solid waste for heavy metals adsorption features and challenges; a review, J. Mater. Res. Technol. 9 (2020) 10235–10253. https://doi.org/10.1016/j.jmrt.2020.07.045.

[6] X. Wang, X. Liang, Y. Wang, X. Wang, M. Liu, D. Yin, S. Xia, J. Zhao, Y. Zhang, Adsorption of Copper (II) onto activated carbons from sewage sludge by microwave-induced phosphoric acid and zinc chloride activation, Desalination. 278 (2011) 231–237. https://doi.org/10.1016/j.desal.2011.05.033.

[7] H.M. Zwain, M. Vakili, I. Dahlan, Waste material adsorbents for zinc removal from wastewater: A comprehensive review, Int. J. Chem. Eng. 2014 (2014). https://doi.org/10.1155/2014/347912.

[8] V.J. Landin-Sandoval, D.I. Mendoza-Castillo, A. Bonilla-Petriciolet, I.A. Aguayo-Villarreal, H.E. Reynel-Avila, H.A. Gonzalez-Ponce, Valorization of agri-food industry wastes to prepare

adsorbents for heavy metal removal from water, J. Environ. Chem. Eng. 8 (2020) 104067. https://doi.org/10.1016/j.jece.2020.104067.

[9] C. Namasivayam, K. Kadirvelu, Agricultural solid wastes for the removal of heavy metals: Adsorption of Cu(II) by coirpith carbon, Chemosphere. 34 (1997) 377–399. https://doi.org/10.1016/S0045-6535(96)00384-0.

[10] C. Roy, A. Dutta, M. Mahapatra, M. Karmakar, J.S.D. Roy, M. Mitra, P.K. Chattopadhyay, N.R. Singha, Collagenic waste and rubber based resin-cured biocomposite adsorbent for high-performance removal(s) of Hg(II), safranine, and brilliant cresyl blue: A cost-friendly waste management approach, J. Hazard. Mater. 369 (2019) 199–213. https://doi.org/10.1016/j.jhazmat.2019.02.004.

[11] N.R. Singha, C. Roy, M. Mahapatra, A. Dutta, J.S. Deb Roy, M. Mitra, P.K. Chattopadhyay, Scalable Synthesis of Collagenic-Waste and Natural Rubber-Based Biocomposite for Removal of Hg(II) and Dyes: Approach for Cost-Friendly Waste Management, ACS Omega. 4 (2019) 421–436. https://doi.org/10.1021/acsomega.8b02799.

[12] R. Shahrokhi-Shahraki, C. Benally, M.G. El-Din, J. Park, High efficiency removal of heavy metals using tire-derived activated carbon vs commercial activated carbon: Insights into the adsorption mechanisms, Chemosphere. 264 (2021) 128455. https://doi.org/10.1016/j.chemosphere.2020.128455.

[13] M.E. Mahmoud, M.M. Saleh, M.M. Zaki, G.M. Nabil, A sustainable nanocomposite for removal of heavy metals from water based on crosslinked sodium alginate with iron oxide waste material from steel industry, J. Environ. Chem. Eng. 8 (2020) 104015. https://doi.org/10.1016/j.jece.2020.104015.

[14] V.M. Monsalvo, A.F. Mohedano, J.J. Rodriguez, Adsorption of 4-chlorophenol by inexpensive

sewage sludge-based adsorbents, Chem. Eng. Res. Des. 90 (2012) 1807–1814. https://doi.org/10.1016/j.cherd.2012.03.018.

[15] J. Wang, S. Wang, Preparation, modification and environmental application of biochar: A review, J. Clean. Prod. 227 (2019) 1002–1022. https://doi.org/10.1016/j.jclepro.2019.04.282.

[16] F. Rozada, L.F. Calvo, A.I. García, J. Martín-Villacorta, M. Otero, Dye adsorption by sewage sludge-based activated carbons in batch and fixed-bed systems, Bioresour. Technol. 87 (2003) 221–230. https://doi.org/10.1016/S0960-8524(02)00243-2.

[17] H. Lu, W. Zhang, Y. Yang, X. Huang, S. Wang, R. Qiu, Relative distribution of Pb 2+ sorption mechanisms by sludge-derived biochar, Water Res. 46 (2012) 854–862. https://doi.org/10.1016/j.watres.2011.11.058.

[18] E. Silva, G. Caixeta, T. Borges, M. Mendes, L. Carrijo, A. Melo, R. Guimarães, L. Roberto, G. Guilherme, Ecotoxicology and Environmental Safety Combining biochar and sewage sludge for immobilization of heavy metals in mining soils, Ecotoxicol. Environ. Saf. 172 (2019) 326–333. https://doi.org/10.1016/j.ecoenv.2019.01.110.

[19] X. Chen, S. Jeyaseelan, N. Graham, Physical and chemical properties study of the activated carbon made from sewage sludge, Waste Manag. 22 (2002) 755–760. https://doi.org/10.1016/S0956-053X(02)00057-0.

[20] A. Hammaini, F. González, A. Ballester, M.L. Blázquez, J.A. Muñoz, Biosorption of heavy metals by activated sludge and their desorption characteristics, J. Environ. Manage. 84 (2007) 419–426. https://doi.org/10.1016/j.jenvman.2006.06.015.

[21] S. Wang, W. Guo, F. Gao, R. Yang, Characterization and Pb(II) removal potential of corn straw- and municipal sludge-derived biochars, R. Soc. Open Sci. 4 (2017). https://doi.org/10.1098/rsos.170402.

[22] Y. Xue, C. Wang, Z. Hu, Y. Zhou, Y. Xiao, T. Wang, Pyrolysis of sewage sludge by electromagnetic induction: Biochar properties and application in adsorption removal of Pb(II), Cd(II) from aqueous solution, Waste Manag. 89 (2019) 48–56. https://doi.org/10.1016/j.wasman.2019.03.047.

[23] F. Zhou, H. Wang, S. Fang, W. Zhang, R. Qiu, Pb(II), Cr(VI) and atrazine sorption behavior on sludge-derived biochar: role of humic acids, Environ. Sci. Pollut. Res. 22 (2015) 16031–16039. https://doi.org/10.1007/s11356-015-4818-7.

[24] F. Rozada, M. Otero, A. Morán, A.I. García, Adsorption of heavy metals onto sewage sludge-derived materials, Bioresour. Technol. 99 (2008) 6332–6338. https://doi.org/10.1016/j.biortech.2007.12.015.

[25] W. Zhang, S. Mao, H. Chen, L. Huang, R. Qiu, Pb(II) and Cr(VI) sorption by biochars pyrolyzed from the municipal wastewater sludge under different heating conditions, Bioresour. Technol. 147 (2013) 545–552. https://doi.org/10.1016/j.biortech.2013.08.082.

[26] J. Zhang, J. Shao, Q. Jin, Z. Li, X. Zhang, Y. Chen, S. Zhang, H. Chen, Sludge-based biochar activation to enhance Pb(II) adsorption, Fuel. 252 (2019) 101–108. https://doi.org/10.1016/j.fuel.2019.04.096.

[27] J. Ifthikar, T. Wang, A. Khan, A. Jawad, T. Sun, X. Jiao, Z. Chen, J. Wang, Q. Wang, H. Wang, A. Jawad, Highly Efficient Lead Distribution by Magnetic Sewage Sludge Biochar: Sorption Mechanisms and Bench Applications, Bioresour. Technol. 238 (2017) 399–406. https://doi.org/10.1016/j.biortech.2017.03.133.

[28] X. Huang, D. Wei, X. Zhang, D. Fan, X. Sun, B. Du, Q. Wei, Synthesis of amino-functionalized magnetic aerobic granular sludge-biochar for Pb(II) removal: Adsorption performance and mechanism studies, Sci. Total Environ. 685 (2019) 681–689.

https://doi.org/10.1016/j.scitotenv.2019.05.429.

[29] L. Fan, Y. Chen, L. Wang, W. Jiang, Adsorption of Pb(II) ions from aqueous solutions by pyrolusite-modified activated carbon prepared from sewage sludge, Adsorpt. Sci. Technol. 29 (2011) 495–506. https://doi.org/10.1260/0263-6174.29.5.495.

[30] R. Xie, W. Jiang, J. Peng, Y. Chen, Effect of Pyrolusite Loading on Sewage Sludge-Based Activated Carbon in Cu(II), Pb(II), and Cd(II) Adsorption, Environ. Prog. Sustain. Energy. 32 (2013) 1066–1073. https://doi.org/10.1002/ep.

[31] T. Phuengprasop, J. Sittiwong, F. Unob, Removal of heavy metal ions by iron oxide coated sewage sludge, J. Hazard. Mater. 186 (2011) 502–507. https://doi.org/10.1016/j.jhazmat.2010.11.065.

[32] S. Shi, G. Xu, H. Yu, Z. Zhang, Strategies of valorization of sludge from wastewater treatment, J. Chem. Technol. Biotechnol. 93 (2018) 936–944. https://doi.org/10.1002/jctb.5548.

[33] J. Saleem, U. Bin Shahid, M. Hijab, H. Mackey, G. McKay, Production and applications of activated carbons as adsorbents from olive stones, Biomass Convers. Biorefinery. 9 (2019) 775–802. https://doi.org/10.1007/s13399-019-00473-7.

[34] E. Wolak, E.B. Vogt, J. Szczurowski, Chemical and hydrophobic modification of activated WD-extra carbon, E3S Web Conf. 14 (2017). https://doi.org/10.1051/e3sconf/20171402033.

[35] J. Li, D.H.L. Ng, P. Song, C. Kong, Y. Song, P. Yang, Preparation and characterization of high-surface-area activated carbon fibers from silkworm cocoon waste for congo red adsorption, Biomass and Bioenergy. 75 (2015) 189–200. https://doi.org/10.1016/j.biombioe.2015.02.002.

[36] H. Benhima, M. Chiban, F. Sinan, P. Seta, M. Persin, Removal of lead and cadmium ions from aqueous solution by adsorption onto micro-particles of dry plants, Colloids Surfaces B

Biointerfaces. 61 (2008) 10–16. https://doi.org/10.1016/j.colsurfb.2007.06.024.

[37] J.N. Sahu, S. Agarwal, B.C. Meikap, M.N. Biswas, Performance of a modified multi-stage bubble column reactor for lead(II) and biological oxygen demand removal from wastewater using activated rice husk, J. Hazard. Mater. 161 (2009) 317–324. https://doi.org/10.1016/j.jhazmat.2008.03.094.

[38] K.L. Tan, B.H. Hameed, Insight into the adsorption kinetics models for the removal of contaminants from aqueous solutions, J. Taiwan Inst. Chem. Eng. 74 (2017) 25–48. https://doi.org/10.1016/j.jtice.2017.01.024.

[39] Z. Wang, J. Zhao, L. Song, H. Mashayekhi, B. Chefetz, B. Xing, Adsorption and desorption of phenanthrene on carbon nanotubes in simulated gastrointestinal fluids, Environ. Sci. Technol. 45 (2011) 6018–6024. https://doi.org/10.1021/es200790x.

[40] P.R. Gunjal, V. V. Ranade, Catalytic Reaction Engineering, in: Ind. Catal. Process. Fine Spec. Chem., Elsevier, 2016: pp. 263–314. https://doi.org/10.1016/B978-0-12-801457-8.00007-0.

[41] L. Largitte, R. Pasquier, A review of the kinetics adsorption models and their application to the adsorption of lead by an activated carbon, Chem. Eng. Res. Des. 109 (2016) 495–504. https://doi.org/10.1016/j.cherd.2016.02.006.

[42] R.K. Prasad, S.N. Srivastava, Sorption of distillery spent wash onto fly ash: Kinetics and mass transfer studies, Chem. Eng. J. 146 (2009) 90–97. https://doi.org/10.1016/j.cej.2008.05.021.

[43] H.N. Tran, S.J. You, A. Hosseini-Bandegharaei, H.P. Chao, Mistakes and inconsistencies regarding adsorption of contaminants from aqueous solutions: A critical review, Water Res. 120 (2017) 88–116. https://doi.org/10.1016/j.watres.2017.04.014.

[44] K.Y. Foo, B.H. Hameed, Insights into the modeling of adsorption isotherm systems, Chem. Eng. J. 156 (2010) 2–10. https://doi.org/10.1016/j.cej.2009.09.013.

[45] I. Langmuir, The adsorption of gases on plane surfaces of glass, mica and platinum, J. Am. Chem. Soc. 40 (1918) 1361–1403. https://doi.org/10.1021/ja02242a004.

[46] C.H. Bolster, G.M. Hornberger, On the Use of Linearized Langmuir Equations, Soil Sci. Soc. Am. J. 71 (2007) 1796–1806. https://doi.org/10.2136/sssaj2006.0304.

[47] A.H. Hawari, C.N. Mulligan, Heavy metals uptake mechanisms in a fixed-bed column by calcium-treated anaerobic biomass, Process Biochem. 41 (2006) 187–198. https://doi.org/10.1016/j.procbio.2005.06.018.

[48] Y. Wang, L. Chai, H. Chang, X. Peng, Y. Shu, Equilibrium of hydroxyl complex ions in Pb2+-H2O system, Trans. Nonferrous Met. Soc. China. 19 (2009) 458–462. https://doi.org/10.1016/S1003-6326(08)60295-2.

[49] C.P. Dwivedi, J.N. Sahu, C.R. Mohanty, B.R. Mohan, B.C. Meikap, Column performance of granular activated carbon packed bed for Pb(II) removal, J. Hazard. Mater. 156 (2008) 596–603. https://doi.org/10.1016/j.jhazmat.2007.12.097.

[50] Y. Dai, C. Du, H. Yu, D. Zhang, S. Tanaka, Effect of contact time, solution pH, dosage of adsorbent, and regeneration on adsorption behavior of lead using nitric acid treated carbon material, Fresenius Environ. Bull. 25 (2016) 3493–3506.

[51] N.E. Davila-Guzman, F.J. Cerino-Córdova, M. Loredo-Cancino, J.R. Rangel-Mendez, R. Gómez-González, E. Soto-Regalado, Studies of Adsorption of Heavy Metals onto Spent Coffee Ground: Equilibrium, Regeneration, and Dynamic Performance in a Fixed-Bed Column, Int. J. Chem. Eng. 2016 (2016). https://doi.org/10.1155/2016/9413879.

[52] P. Goyal, P. Sharma, S. Srivastava, M.M. Srivastava, Saraca indica leaf powder for decontamination of Pb: Removal, recovery, adsorbent characterization and equilibrium modeling, Int. J. Environ. Sci. Technol. 5 (2008) 27–34. https://doi.org/10.1007/BF03325994.

[53] A. Lalmi, K.E. Bouhidel, B. Sahraoui, C. el H. Anfif, Removal of lead from polluted waters using ion exchange resin with Ca(NO3)2 for elution, Hydrometallurgy. 178 (2018) 287–293. https://doi.org/10.1016/j.hydromet.2018.05.009.

[54] J.F. d. S.S. Costa, V.J.P. Vilar, C.M.S. Botelho, E.A.B. da Silva, R.A.R. Boaventura, Application of the Nernst-Planck approach to lead ion exchange in Ca-loaded Pelvetia canaliculata, Water Res. 44 (2010) 3946–3958. https://doi.org/10.1016/j.watres.2010.04.033.

[55] B. Volesky, Biosorption and me, Water Res. 41 (2007) 4017–4029. https://doi.org/10.1016/j.watres.2007.05.062.

[56] J. Liang, C. Chen, B.A. Yoza, Y. Liang, J. Li, M. Ke, Q. Wang, Hydrolysis and acidification of activated sludge from a petroleum refinery, Pet. Sci. 16 (2019) 428–438. https://doi.org/10.1007/s12182-019-0301-2.

[57] J. Wang, X. Guo, Adsorption kinetic models: Physical meanings, applications, and solving methods, J. Hazard. Mater. 390 (2020) 122156. https://doi.org/10.1016/j.jhazmat.2020.122156.

[58] X. Guo, J. Wang, A general kinetic model for adsorption: Theoretical analysis and modeling, J. Mol. Liq. 288 (2019) 111100. https://doi.org/10.1016/j.molliq.2019.111100.

[59] R.J. Hyndman, G. Athanasopoulos, Forecasting: principles and practice, OTexts, Heathmont, 2018.

[60] K.L. Muedi, H.G. Brink, V. Masindi, J.P. Maree, Effective removal of arsenate from wastewater using aluminium enriched ferric oxide-hydroxide recovered from authentic acid mine drainage, J. Hazard. Mater. (2021) 125491. https://doi.org/10.1016/j.jhazmat.2021.125491.

[61] Z. Liu, Y. Huang, G. Zhao, Preparation and characterization of activated carbon fibers from

liquefied wood by ZnCl2 activation, BioResources. 11 (2016) 3178–3190. https://doi.org/10.15376/biores.11.2.3178-3190.

[62] K. Sears, J.E. Alleman, J.L. Barnard, J.A. Oleszkiewicz, Density and Activity Characterization of Activated Sludge Flocs, J. Environ. Eng. 132 (2006) 1235–1242. https://doi.org/10.1061/(asce)0733-9372(2006)132:10(1235).

[63] E. Smidt, P. Lechner, M. Schwanninger, G. Haberhauer, M.H. Gerzabek, Characterization of waste organic matter by FT-IR spectroscopy: Application in waste science, Appl. Spectrosc. 56 (2002) 1170–1175. https://doi.org/10.1366/000370202760295412.

[64] O. Francioso, M.T. Rodriguez-Estrada, D. Montecchio, C. Salomoni, A. Caputo, D. Palenzona, Chemical characterization of municipal wastewater sludges produced by two-phase anaerobic digestion for biogas production, J. Hazard. Mater. 175 (2010) 740–746. https://doi.org/10.1016/j.jhazmat.2009.10.071.

[65] J. De Oliveira Silva, G.R. Filho, C. Da Silva Meireles, S.D. Ribeiro, J.G. Vieira, C.V. Da Silva, D.A. Cerqueira, Thermal analysis and FTIR studies of sewage sludge produced in treatment plants. the case of sludge in the city of Uberlândia-MG, Brazil, Thermochim. Acta. 528 (2012) 72–75. https://doi.org/10.1016/j.tca.2011.11.010.

[66] M. Grube, J.G. Lin, P.H. Lee, S. Kokorevicha, Evaluation of sewage sludge-based compost by FT-IR spectroscopy, Geoderma. 130 (2006) 324–333. https://doi.org/10.1016/j.geoderma.2005.02.005.

[67] J. Coates, Interpretation of Infrared Spectra, A Practical Approach, Encycl. Anal. Chem. (2006). https://doi.org/10.1002/9780470027318.a5606.

[68] S. Amir, M. Hafidi, G. Merlina, H. Hamdi, J.-C. Revel, Elemental analysis, FTIR and 13C-NMR of humic acids from sewage sludge composting., Agronomie. 24 (2004) 13–18.

https://doi.org/10.1051/agro:2003054.

[69] L. Vidal, E. Joussein, M. Colas, J. Cornette, J. Sanz, I. Sobrados, J.L. Gelet, J. Absi, S. Rossignol, Controlling the reactivity of silicate solutions: A FTIR, Raman and NMR study, Colloids Surfaces A Physicochem. Eng. Asp. 503 (2016) 101–109. https://doi.org/10.1016/j.colsurfa.2016.05.039.

[70] B.L. Guo, Y.H. Chen, X.J. Liu, W.C. Liu, A.D. Li, Optical and electrical properties study of sol-gel derived Cu2ZnSnS4 thin films for solar cells, AIP Adv. 4 (2014). https://doi.org/10.1063/1.4895520.

[71] H. Bhunia, B. Kundu, S. Chatterjee, A.J. Pal, Heterovalent substitution in anionic and cationic positions of PbS thin-films grown by SILAR method vis-à-vis Fermi energy measured through scanning tunneling spectroscopy, J. Mater. Chem. C. 4 (2016) 551–558. https://doi.org/10.1039/c5tc03959b.

[72] M. Bhaumik, A. Maity, H.G. Brink, Zero valent nickel nanoparticles decorated polyaniline nanotubes for the efficient removal of Pb(II) from aqueous solution: Synthesis, characterization and mechanism investigation, Chem. Eng. J. (2020) 127910. https://doi.org/10.1016/j.cej.2020.127910.

[73] D. Tan, Z. Ma, B. Xu, Y. Dai, G. Ma, M. He, Z. Jin, J. Qiu, Surface passivated silicon nanocrystals with stable luminescence synthesized by femtosecond laser ablation in solution, Phys. Chem. Chem. Phys. 13 (2011) 20255–20261. https://doi.org/10.1039/c1cp21366k.

[74] R.J.J. Jansen, H. van Bekkum, XPS of nitrogen-containing functional groups on activated carbon, Carbon N. Y. 33 (1995) 1021–1027. https://doi.org/10.1016/0008-6223(95)00030-H.

[75] R. Karmakar, S. Bindiya, P. Hariprasad, Convergent evolution in bacteria from multiple origins under antibiotic and heavy metal stress, and endophytic conditions of host plant, Sci.

Total Environ. 650 (2019) 858–867. https://doi.org/10.1016/j.scitotenv.2018.09.078.

[76] M. Mitra, M. Mahapatra, A. Dutta, J.S.D. Roy, M. Karmakar, M. Deb, H. Mondal, P.K. Chattopadhyay, A. Bandyopadhyay, N.R. Singha, Carbohydrate and collagen-based doubly-grafted interpenetrating terpolymer hydrogel via N–H activated in situ allocation of monomer for superadsorption of Pb(II), Hg(II), dyes, vitamin-C, and p-nitrophenol, J. Hazard. Mater. 369 (2019) 746–762. https://doi.org/10.1016/j.jhazmat.2018.12.019.

[77] R. hong Liang, Y. Li, L. Huang, X. dong Wang, X. xue Hu, C. mei Liu, M. shun Chen, J. Chen, Pb2+ adsorption by ethylenediamine-modified pectins and their adsorption mechanisms, Carbohydr. Polym. 234 (2020). https://doi.org/10.1016/j.carbpol.2020.115911.

[78] D.J. Fletouris, Clean-up and fractionation methods, Woodhead Publishing Limited, 2007. https://doi.org/10.1016/B978-044452843-8/50011-0.

[79] J. Wang, X. Guo, Adsorption isotherm models: Classification, physical meaning, application and solving method, Chemosphere. 258 (2020) 127279. https://doi.org/10.1016/j.chemosphere.2020.127279.

[80] S. Wang, J.H. Kwak, M.S. Islam, M.A. Naeth, M. Gamal El-Din, S.X. Chang, Biochar surface complexation and Ni(II), Cu(II), and Cd(II) adsorption in aqueous solutions depend on feedstock type, Sci. Total Environ. 712 (2020) 136538. https://doi.org/10.1016/j.scitotenv.2020.136538.

[81] T.G. Ambaye, M. Vaccari, E.D. van Hullebusch, A. Amrane, S. Rtimi, Mechanisms and adsorption capacities of biochar for the removal of organic and inorganic pollutants from industrial wastewater, Int. J. Environ. Sci. Technol. (2020). https://doi.org/10.1007/s13762-020-03060-w.

[82] H. Li, X. Dong, E.B. da Silva, L.M. de Oliveira, Y. Chen, L.Q. Ma, Mechanisms of metal

sorption by biochars: Biochar characteristics and modifications, Chemosphere. 178 (2017) 466–478. https://doi.org/10.1016/j.chemosphere.2017.03.072.

[83] J.J. Salazar-Rabago, R. Leyva-Ramos, Novel biosorbent with high adsorption capacity prepared by chemical modification of white pine (Pinus durangensis) sawdust. Adsorption of Pb(II) from aqueous solutions, J. Environ. Manage. 169 (2016) 303–312. https://doi.org/10.1016/j.jenvman.2015.12.040.

[84] S. Kumar, S. Jain, History , Introduction , and Kinetics of Ion Exchange Materials, J. Chem. 2013 (2013). https://doi.org/http://dx.doi.org/10.1155/2013/957647 Review.

[85] M. Trgo, J. Perić, Interaction of the zeolitic tuff with Zn-containing simulated pollutant solutions, J. Colloid Interface Sci. 260 (2003) 166–175. https://doi.org/10.1016/S0021-9797(03)00042-0.

[86] Z. Hubicki, D. Kołodyńska, Selective Removal of Heavy Metal Ions from Waters and Waste Waters Using Ion Exchange Methods, in: Ion Exch. Technol., IntechOpen, 2012: pp. 193–240. https://doi.org/http://dx.doi.org/10.5772/51040.

[87] K.L. Timofeev, S.S. Naboichenko, Mechanism of sorption equilibrium in the recovery of zinc, calcium, and magnesium from waste water by the use of iminodiacetate resins, Metallurgist. 57 (2013) 95–99. https://doi.org/10.1007/s11015-013-9697-x.

[88] Bio-Rad Laboratories, Chelex 100 Chelating Ion Exchange Resin Instruction Manual, Bio-Rad Lab. (2017) 1–24.

[89] D. Clifford, T. Sorg, G. Ghurye, Ion exchange and adsorption of inorganic contaminants, in: Water Qual. Treat. A Handb. Drink. Water, Sixth Edit, McGraw-Hill Professional, 2011. https://doi.org/10.1002/047147844X.pc1506.

[90] S.E. Jørgensen, Adsorption and Ion Exchange, in: Dev. Environ. Model., 1989: p. 65.

https://doi.org/https://doi.org/10.1016/B978-0-444-88030-7.50003-2.

[91] W. Cheng, C. Liu, T. Tong, R. Epsztein, M. Sun, R. Verduzco, Selective removal of divalent cations by polyelectrolyte multilayer nanofiltration membrane : Role of polyelectrolyte charge , ion size , and ionic strength Selective removal of divalent cations by polyelectrolyte multilayer nano fi ltration membrane : Ro, J. Memb. Sci. 559 (2018) 98–106. https://doi.org/10.1016/j.memsci.2018.04.052.

[92] E.R. Nightingale, Phenomenological theory of ion solvation. Effective radii of hydrated ions, J. Phys. Chem. 63 (1959) 1381–1387. https://doi.org/10.1021/j150579a011.

[93] S.M. Tichapondwa, J.P. Newman, O. Kubheka, Effect of TiO2 phase on the photocatalytic degradation of methylene blue dye, Phys. Chem. Earth. 118–119 (2020) 102900. https://doi.org/10.1016/j.pce.2020.102900.

[94] C.H. Weng, P.C. Chiang, E.E. Chang, Adsorption characteristics of CuII on to industrial wastewater sludges, Adsorpt. Sci. Technol. 19 (2001) 143–157. https://doi.org/10.1260/0263617011494042.

[95] C.P. Huang, J. Wang, Specific chemical interactions between metal ions and biological solids exemplified by sludge particulates, Bioresour. Technol. 160 (2014) 32–42. https://doi.org/10.1016/j.biortech.2014.01.043.

[96] S. Li, Y. Yao, T. Zhao, M. Wang, F. Wu, Biochars preparation from waste sludge and composts under different carbonization conditions and their Pb(II) adsorption behaviors, Water Sci. Technol. 80 (2019) 1063–1075. https://doi.org/10.2166/wst.2019.353.